The effect of aluminum and platinum additives on hydrogen adsorption on mesoporous silicates

Journal:	*Physical Chemistry Chemical Physics*
Manuscript ID	CP-ART-10-2017-007015.R1
Article Type:	Paper
Date Submitted by the Author:	01-Apr-2018

Complete List of Authors:	Melaet , Gerome; University of California Berkeley Stavila, Vitalie; Sandia National Laboratories, Engineered Materials Department, MS-9161 Klebanoff , Lennie ; Sandia National Laboratories California Somorjai, Gabor; University of California at Berkeley, Chemistry

The effect of aluminum and platinum additives on hydrogen adsorption on mesoporous silicates

Gérôme Melaet,[a] Vitalie Stavila,[b*] Lennie Klebanoff,[b] and Gabor A. Somorjai[a,c*]

[a] *Materials Science Division, Lawrence Berkeley National Laboratory, Berkeley CA 94720*

[b] *Sandia National Laboratories, Livermore CA 94551 USA*

[c] *Department of Chemistry, University of California-Berkeley, Berkeley CA 94720*

Abstract

Recent theoretical predictions indicate that functional groups and additives could have a favorable impact on the hydrogen adsorption characteristics of sorbents; however, no definite evidence has been obtained to date and little is known about the impact of such modifications on the thermodynamics of hydrogen uptake and overall capacity. In this work, we investigate the effect of two types of additives on the cryoadsorption of hydrogen to mesoporous silica. First, Lewis and Brønsted acid sites were evaluated by grafting aluminum to the surface of mesoporous silica (MCF-17) and characterizing the resulting silicate materials surface area and the concentration of Brønsted and Lewis acid sites created. Heat of adsorption measurements found little influence of surface acidity on the enthalpy of hydrogen cryoadsorption. Secondly, platinum nanoparticles of 1.5 nm and 7.1 nm in diameter were loaded into MCF-17, and characterized by TEM. Hydrogen absorption measurements revealed that the addition of small amounts of metallic platinum nanoparticles increases by up to two-fold the amount of hydrogen adsorbed at liquid nitrogen temperature. Moreover, we found a direct correlation between the size of platinum particles and the amount of hydrogen stored, in favor of smaller particles.

* Corresponding authors:
Dr. Vitalie Stavila (vnstavi@sandia.gov) and Prof. Gabor A. Somorjai (somorjai@berkeley.edu)

1. Introduction

Hydrogen-based technologies can provide the basis for reducing our societal dependence on dwindling fossil fuel reserves, significantly decrease greenhouse gas (GHG) emissions, and achieve a more secure energy future.[1] In this way, the use of hydrogen as a fuel would be beneficial at both the environmental and geopolitical levels. As described by Klebanoff *et al.*,[2] proton exchange membrane (PEM) fuel-cells that convert hydrogen chemical energy into electrical power are already finding use in the first fuel-cell vehicles, and also commercial use in portable power, telecom backup power, material handling equipment and fuel-cell mobile lighting. A considerable amount of research has been devoted to various methods of storing hydrogen for these disparate applications. For light-duty fuel-cell vehicles, the current commercially available vehicles use fully wrapped high strength carbon fiber (type III or IV) pressure vessels[3] storing compressed hydrogen gas at 350 or 700 bar.[4]

While allowing the roll-out of the first hydrogen fuel-cell vehicles, high pressure storage of hydrogen limits the range of these vehicles, which could be improved by finding storage methods with higher gravimetric and volumetric storage densities. The hydrogen storage density can be improved by exploiting the attractive forces between hydrogen and other atoms through chemical binding to other elements in complex metal hydrides,[5,6] chemical hydrides,[7,8] inside a solid metallic matrix as atoms in interstitial metal hydrides[9,10] or by physisorption on large surface area materials.[11,12] Here, we focus on physisorption of molecular hydrogen on large surface area materials at cryogenic temperature, an approach called cryoadsorption.

Cryoadsorption is based on the binding of H_2 molecules to porous solids with large surface areas (*i.e.*, usually greater than 500 m^2/g). Most attention has been focused on activated carbons and metal-organic framework (MOF) compounds, although nanocarbons, zeolites, microporous polymers, and other materials have also been actively investigated over the past two decades.[11,12] Since adsorption bonding arises from relatively weak van der Waals attractions of the H_2 molecules to the sorbent surfaces, the enthalpies of molecular adsorption are usually ~ 2 – 10 kJ/mole H_2 (in the physisorption range). This requires the sorbent material to be cooled to cryogenic temperatures (e.g. < 100 K) for significant hydrogen storage capacities to be realized, which is a practical inconvenience with added system complexity and cost. It is believed that an enthalpy of desorption of ~ 15-20 kJ/mole H_2 is optimal for the light-duty fuel-cell vehicle

application, which would enable hydrogen storage near room temperature. Petitpas and co-workers have recently reported a detailed thermodynamic analysis of the cryoadsorption hydrogen storage method.[13]

The use of cryo-adsorption for hydrogen storage for fuel-cell vehicles has been analyzed in an engineering sense, comparing a hydrogen storage system based on adsorption with the FreedomCAR/Fuel Technical Targets.[14] While the primary deficiencies of the cryoadsorption approach are the gravimetric and volumetric storage densities, such a system is attractive from other standpoints such as cycle life, fuel purity and kinetic response. The work presented here is directed to improving the storage density of adsorption systems through chemical additives, in particular additives that may increase the gas-solid interaction in the physisorption regime.

We choose mesoporous silica as a substrate for this study, as this material can be easily functionalized in various ways. Prior hydrogen adsorption studies have been reported for undoped mesoporous silica,[15,16] zeolites based on the silica backbone[17,18] and clusters supported on silica substrates.[19,20] Although the hydrogen storage capacity of mesoporous silica itself is unremarkable, this material serves as a convenient model system whose surface can be selectively modified. In particular, mesoporous silica type MCF-17, a high surface area material commonly used in academic research as a catalyst support, can be modified with different elements through a grafting procedure in order to give functionality to the silica surface while maintaining the structural integrity of the framework. Modifying mesoporous silica with Al introduces high concentrations of strong acid sites to the high-surface area material, thereby providing a conceptual path to a high-capacity catalytically tuned hydrogen storage material, if acid sites indeed promoted hydrogen adsorption.

Thus, we seek to understand if modifying surface acidity of high surface area (i.e. 10^2-10^3 m^2/g) mesoporous silica improves the physisorption storage capacity or increase hydrogen's heat of adsorption on the grafted silica surface. Several past studies focused on the effect of surface acidity on the hydrogen sorption capacity of activated carbon.[21,22] However, little information was provided about the nature of the acid sites, possibly due to the relatively complex pore structure of the carbons. In this study, we selected a well-defined silica substrate to assess both Brønsted acid and Lewis acid functionality on the hydrogen physisorption. Through these experiments, we evaluate if creation of a Lewis acid site, that can accept electron density from

molecular hydrogen, can increase the adsorption energy. Similarly, we evaluate if a Brønsted acid site, which increases the local gradient of electric charge, can polarize an incoming hydrogen molecule, thereby increasing molecular hydrogen adsorption. In addition, we explore the addition of Pt to mesoporous silica, and compare the results with prior studies of Pt nanoparticles (NPs) on activated carbon,[23] Pd NPs on carbon template composites[24] and Ni nanoparticles on carbon nanotubes.[25] Thus, the mesoporous silica allows study of three distinct types of additives: Brønsted acid sites, Lewis acid sites and metallic sites. The strategy for introducing acid sites onto the mesoporous silica is shown in Figure 1.

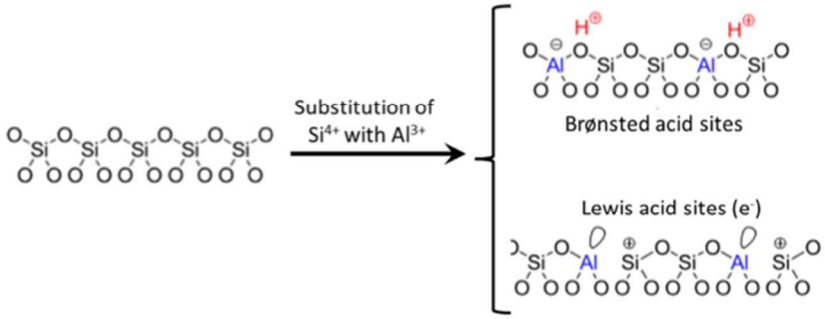

Figure 1. Introduction of surface Brønsted Acid and Lewis Acid sites via grafting aluminum onto the silica surface.

In this approach, aluminum is substitutionally grafted onto the silica surface,[26,27] forming 3-fold coordinate and 4-fold coordinate Al sites. Note that this is a surface functionalization, distinct from Al-Si zeolites in which Al is distributed throughout the silica backbone. The unoccupied 3p orbital at the 3-fold Al sites can accept electrons, thereby acting as electron-accepting Lewis acid sites. For 4-fold coordinated Al, the aluminum creates a surface anionic complex with oxygen ($[AlO_4]^-$) that can bind protons, forming strong Brønsted acid sites. Both types of acid sites exist on the surface at the same time with varying populations that can be quantified. Previous work on the hydrogenation of ethylene[28] has shown that Pt nanoparticles supported on mesoporous silica have high catalytic activity. We use this system as a test of enhanced binding of H_2 in the cryoadsorption regime via introduction of metal sites.

2. Experimental

Synthesis of MCF-17, Al-modified Al-MCF-17, and Pt Nanoparticles:

In the present study, mesoporous silica was prepared using a sol-gel route as described elsewhere.[29-31] Briefly, 1,3,5-trimethylbenzene (TMB), a pore swelling agent, HCl and a triblock copolymer (Pluronic P123) are combined in solution and stirred for 2 hours at 40 ˚C. Subsequently, TEOS (tetraethyl orthosilicate) is added to the solution with stirring for an additional 20 hours. The sol-gel is then produced by adding NH_4F and raising the temperature to 100 ˚C. After 24 hours of aging at 100 ˚C, the solution is cooled to room temperature and the resulting solid is filtered and calcined at 550 ˚C in air for 4 hours. Nitrogen physisorption measurements confirmed the mesostructured MCF-17 silica with an average pore diameter of 16 nm and a total surface area of ~ 600 m^2/g.

The introduction of Lewis and Brønsted acid sites is achieved by grafting alumina onto the silica structure using a well-established method.[26,27] Briefly, MCF-17 is aluminated by making a slurry of the solid with anhydrous $AlCl_3$ in absolute ethanol. The slurry is stirred overnight and the resulting support is separated from ethanol by rotary evaporation. Finally, the Al-modified MCF-17 (i.e. Al-MCF-17) is dried at 130 ˚C and calcined in air at 550 ˚C. By varying the amount of $AlCl_3$ added to the starting material, we could vary the total amount of aluminum sites in the support and thus vary the amount of Lewis and Brønsted sites. All Al-modified mesoporous materials were further ion-exchanged to the H^+ form to introduce acidic functionality on the aluminosilicate framework (stirred in 1M ammonium nitrate aqueous solution for 6 hours).

Platinum nanoparticles were produced using the colloidal method in the presence of a capping agent. Briefly, a platinum salt (H_2PtCl_4 or H_2PtCl_6) is dissolved in a diol solution. Upon heating, the platinum ions are reduced to metal triggering a mass nucleation. Using this technique, adapted from the literature,[32-34] we prepared two sizes of Pt nanoparticles with 1.5, and 7.5 nm particle diameter. Subsequently, the particles were loaded onto MCF-17 by sonication, as shown schematically in Figure 2.

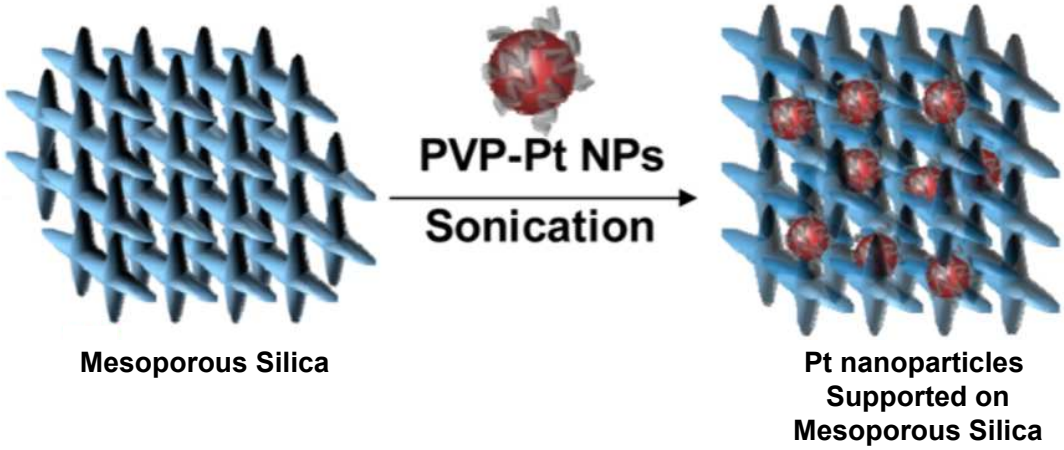

Figure 2. General scheme of platinum nanoparticle loading into mesoporous silica by sonication of Pt NPs colloidal solution with mesoporous silica.

Surface area and hydrogen cryoadsorption measurements:

Specific surface area (SSA) measurements were performed with a Micromeritics ASAP 2020 porosimeter using nitrogen as the probe molecule. The total surface area of the samples was evaluated by the Brunauer-Emmett-Teller method, whereas the average pore size was determined using the Barret-Joyner-Halenda algorithm of the desorption branch of the isotherm. The micropores total volume is derived from the t-plot method.

Hydrogen uptake isotherms were obtained on a few hundred milligrams of sample using a Micromeretics ASAP 2020 (i.e. same system as for the SSA measurements) at liquid nitrogen temperature. The samples were evacuated on the degas port to remove the water contained in the sample (450 ˚C for pure oxide, 150 ˚C for Pt loaded material) prior to uptake measurements. Temperature-dependent hydrogen uptake measurements provided the heat of adsorption.

To obtain accurate measurement of hydrogen uptake on the samples at elevated temperature, ca. in the range of -50 ˚C to -90 ˚C (Julambo chiller), we proceeded with 3 to 4 grams of sample. After each isotherm measurement, the sample was kept on the analysis port where it was degassed under vacuum at 450 ˚C in order to remove any physisorbed hydrogen from the previous experiment. After evacuation at high temperature, the sample was allowed to cool down under vacuum, and the partial pressure in the reactor is recorded before the next experiment (2 μbar). Subsequently, the isosteric heat of adsorption for hydrogen is evaluated at constant coverage using the following relationship:

$$\Delta H_{ad} = -R\left[\frac{\partial ln(p)}{\partial(T^{-1})}\right]_{\theta} \qquad \text{Equation 1}$$

where ΔH_{ad} is defined as the isosteric heat (enthalpy) of adsorption, R is the gas constant, p is the pressure, T is the temperature, and θ is the coverage ($0 < \theta < 1$, 1 corresponding to a full monolayer). In practice, for a constant coverage, ln(p) is plotted against 1/T and yields a straight line for which the slope is equal to $^{\Delta H_{ad}}/_{R}$.

Transmission Electron Spectroscopy:

Transmission electron microscopy (TEM) measurements of the nanoparticle samples were performed using a JEOL JEM2100F TEM operated at 200 kV. Samples for TEM measurements were prepared by drying a drop of diluted colloid dispersion of the synthesized nanoparticles on a commercial TEM grids. A sample of 200 nanoparticles was used to evaluate the size distributions of the nanoparticles.

3. Results and Discussion

Effect of Acid Sites on Hydrogen Adsorption

To evaluate the effect of acid sites on the adsorption of hydrogen, we have produced three samples; pure MCF-17 (with no acid sites), Al-MCF-17-A (10:1) and Al-MCF-17-B (40:1) where the ratio in parenthesis refers to the nominal ratio of Si to Al in the structure, to be determined by experiment. Thus, we have produced two different samples, one highly concentrated in surface aluminum where we have nominally 10 silicon atoms to one aluminum atom, and a low concentration sample with nominally 40 Si atoms for one 1 aluminum atom. ICP experiments allowed us to evaluate the actual Si:Al ratio in the silicate mesostructure, while pyridine adsorption was performed to evaluate the concentration of Lewis and Brønsted sites in the Al-MCF-17 samples. Using a molar extinction coefficient of 1.13 cm/μmol for Brønsted sites and 1.28 cm/μmol for the Lewis sites (see Supplementary Information for details), we were able

to determine the concentration of each site in the different samples. Figure 3 shows the pyridine FTIR data, and Table 1 reports the results for actual Si:Al ratios, material surface areas and the amounts of Lewis and Brønsted sites created on the surface of mesoporous MCF-17.

Table 1. Physical characteristics of the mesoporous silica samples including the ratio of Si:Al, surface area, Lewis and Brønsted site concentration.

Samples	Nominal Ratio (Si:Al)	Actual Ratio (Si:Al)	SSA (m^2/g)	[Lewis] (μmol/g)	[Brønsted] (μmol/g)
MCF-17	N/A	N/A	622.1	N/A	N/A
Al-MCF-17-A	10:1	11:1	498.5	198.1	238.8
Al-MCF-17-B	40:1	57:1	322.8	151.9	161.5

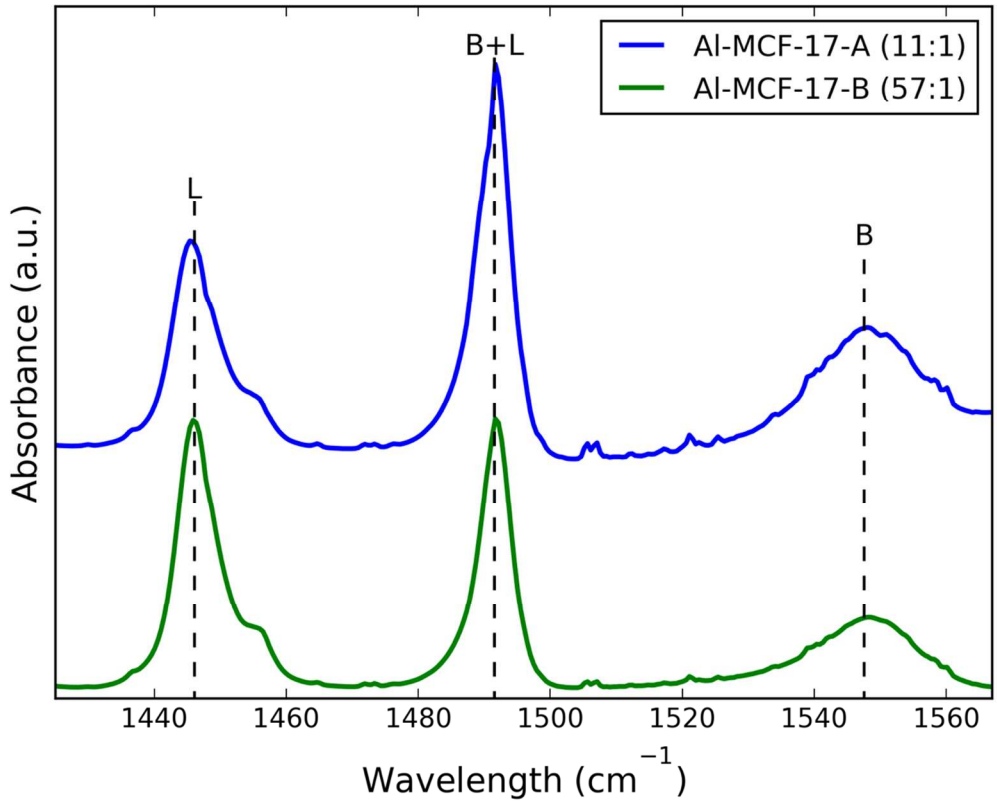

Figure 3. Quantification of Lewis and Brønsted acid site in Al-MCF-17 samples, FTIR absorbance spectra of pyridine adsorbed on Al-MCF-17-A (top curve) and Al-MCF-17-B

(bottom curve), the letters B & L indicate wavelength specific pyridine adsorption on Brønsted and Lewis sites, respectively. FTIR measurements of MCF-17 indicated no pyridine is present.

Pyridine adsorption shows a higher concentration of acid sites for both Lewis and Brønsted types for the "high" Al concentration sample Al-MCF-17-A compared to the "low" Al concentration sample Al-MCF-17-B. The fractional surface coverage of Lewis/Brønsted acid sites is estimated to be 7.1 10^{-3}/8.6 10^{-3} for Al-MCF-17-A and 8.4 10^{-3}/9.0 10^{-3} for Al-MCF-17-B. Hydrogen adsorption isotherms were measured for these samples at liquid nitrogen temperature (-196 ˚C). The results for total amount of H_2 absorbed versus pressure are presented in Figure 4.

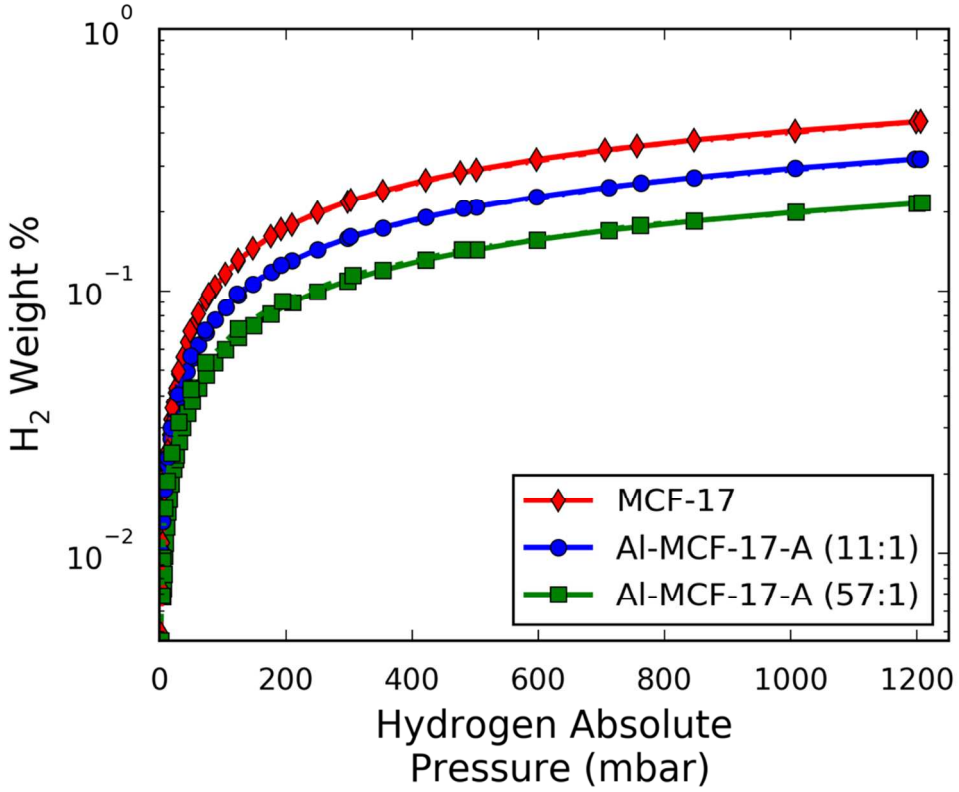

Figure 4. Hydrogen uptake measurements performed at -196 ˚C (liquid nitrogen) comparing three samples: pure MCF-17, Al-MCF-17-A (11:1) and Al-MCF-17-B (57:1).

Rather surprisingly, the isotherm data shows a decrease in the total uptake of hydrogen as a function of the number of acid sites. However, upon a closer examination, it becomes evident that most of the loss in hydrogen adsorption can be directly linked to the reduction in the total

surface area due to the presence of acid sites. Therefore, we compared the samples in terms of surface coverage, dividing the surface area occupied by 1 hydrogen molecule (ca. 0.124 nm^2)[35,36] per the total surface area of the sample (implicitly assuming that we can form a monolayer of H_2). The results of this normalization are presented in Figure 5.

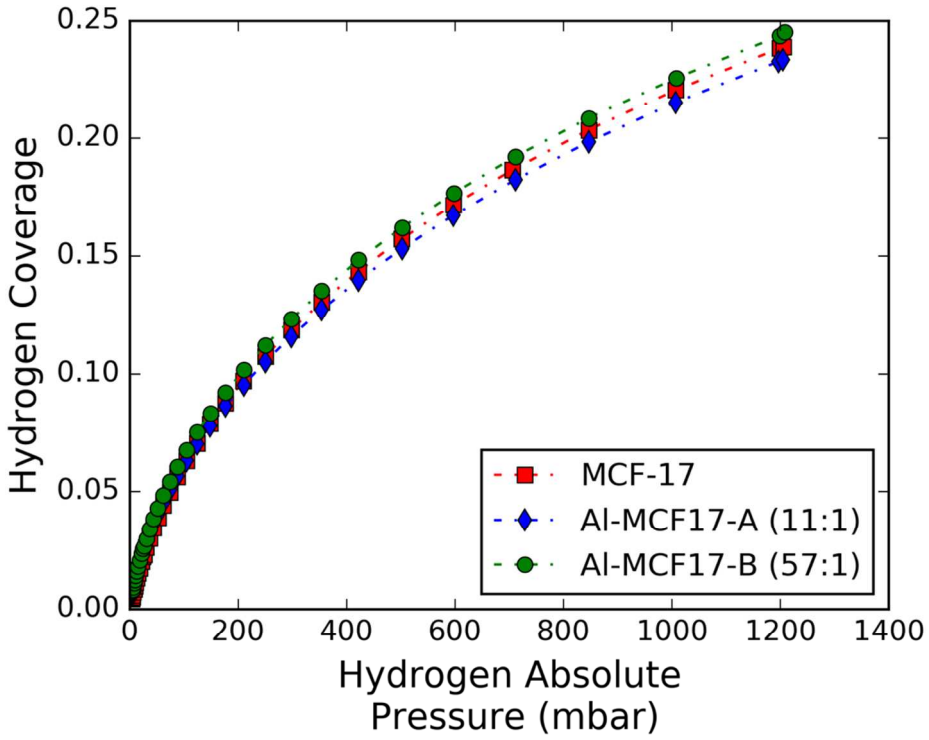

Figure 5. Surface-area normalized hydrogen adsorption in term of hydrogen coverage on the different supports.

As we can see from Figure 5, the intrinsic coverage of hydrogen is the same for each sample, with a maximum of θ = 0.25 at atmospheric pressure. This finding already indicates that the presence of acid sites, either Brønsted or Lewis sites, has little effect on hydrogen cryoadsorption. Kazansky *et al.* measured the -196 ˚C hydrogen adsorption isotherms for a series of isostructural sodium-based faujasite zeolites with different Si/Al ratio.[37] The hydrogen capacity increased in the following order: NaY (Si/Al = 2.4, 56 Na^+ cations per unit cell) < NaX (Si/Al = 1.4, 80 Na^+ cations per unit cell) < NaX (Si/Al = 1.2, 94 Na^+ cations per unit cell) < NaX (Si/Al = 1.05, 87 Na^+ cations per unit cell). As expected, there is a direct correlation between the number of sodium cations in the faujasite structure and the number of sodium ions in the unit cell. However, when normalized by the number of sodium ions present, the authors

found that the amount of hydrogen adsorbed increased with decreasing Si/Al ratios, *i.e.* the introduction of more aluminum sites within the zeolite structure enhances the hydrogen uptake. DRIFTS spectra indicate that the increase of aluminum content in the framework results in larger low-frequency shifts of the hydrogen stretching bands, consistent with the stronger adsorption of hydrogen on these zeolites. The authors hypothesize that, in addition to the sodium sites, the negatively charged oxygen atoms of the zeolite framework contribute significantly to the interactions with hydrogen.

To probe whether the presence of acid influences the enthalpy of hydrogen adsorption ΔH_{ad}, we also measured ΔH_{ad} on these three silica samples. The experiments are performed at low temperatures, between -50 and -90 ˚C, with ΔH_{ad} determined from the slop of ln(p) vs 1/T at a constant coverage (see Equation 1). The absolute values of near-zero coverage heats of adsorption are presented in Table 2.

Table 2. Heat of Adsorption, ΔH_{ad}, at near zero-coverage, as calculated using equation 1.

Sample	ΔH_{ad} (kJ/mol H_2)*
Activated Carbon	8.5
MCF-17	4.5
Al-MCF-17-A (11:1)	4.9
Al-MCF-17- B (57:1)	2.9

**Absolute values of ΔH_{ad} are shown. Since the hydrogen adsorption is an exothermic process, the actual ΔH_{ad} values are negative.*

To confirm the validity of our experimental approach of using a low-pressure (1 atm) system and temperatures above cryogenic temperatures to determine ΔH_{ad}, we first calibrated our method by measuring ΔH_{ad} for a known sample of activated carbon. Our data indicate that ΔH_{ad} for this sample of carbon is 8.5 kJ/mol H_2, which is in good agreement with the literature value for this type of samples (9 kJ/mol H_2).[38] With the method thus validated, we measured the enthalpy of adsorption of hydrogen for MCF-17, obtaining the value 4.5 kJ/mole H_2. This value serves as a reference to compare the effect of surface acidification on the binding of hydrogen to mesoporous silica.

Table 2 shows that neither the Lewis nor Brønsted sites produced concurrently by aluminum grafting significantly increases the enthalpy of cryoadsorption ΔH_{ad} of hydrogen to the mesoporous silicate. The sample with the highest acid content, Al-MCF-17-A (11:1) has a ΔH_{ad} value of 4.9 kJ/mole H_2, slightly higher than that observed for pure MCF-17 (4.5 kJ/mole H_2). The less acidified sample Al-MCF-17-B (57:11) gave a ΔH_{ad} value of 2.9 kJ/mole H_2, even less than that for the unacidified mesoporous silica. Although the exact reason for this decrease in ΔH_{ad} is unclear, it is possible that this is due to the differences in Al-clustering in materials with a different content of Al in silica.

It is worth noting that zeolites (aluminosilicate materials) have been reported[39] to have an isosteric heat of adsorption typically in the range of 6 - 7 kJ/mole H_2, although values as high as 15 kJ/mole H_2 have been observed.[40] Our results suggest that this is mostly due to the smaller physical confinement of microporous zeolite versus the larger mesopores of the Al-MCF-17 samples synthesized and examined in our study. In fact, the existence of micropores is widely accepted to be an important factor in the adsorption of hydrogen, whereas mesopores do not promote H_2 adsorption.

Summarizing the surface acidification portion of this work, we found that surface acidification with either Brønsted or Lewis acid sites does not significantly enhance hydrogen cryoadsorption to mesoporous silicate, and the associated ΔH_{ad} associated with these acid sites fall well below the value ~ 15-20 kJ/mole H_2 needed for practical hydrogen sorption storage systems to operate near room temperature. The lack of surface acidity influence found here for mesoporous silica runs counter to the positive influence of surface acidity found for activated carbon samples,[23-25] where classic acidic moieties such as carboxylic acid were reported to promote hydrogen binding.

The different behavior of acid-site functionalized mesoporous silica and microporous carbons could be explained by the significant difference in pore sizes. It is well known that only micropores (pore sizes less than 2 nm) are efficient for hydrogen storage, whereas pores above 2 nm do not contribute much toward hydrogen adsorption at 77 K.[41] In fact, most of the studies suggest the pore sizes smaller than 1 nm are the most efficient in promoting strong H_2-surface interactions.[42] It is believed that smaller pores display stronger surface-H_2 interactions due to an efficient overlap of potential fields from both sides of the pores, effectively stabilizing the

hydrogen molecules and trapping them into the small slit spaces. For carbons, the strongest interactions are found for pores of ≈0.6 nm, which results in the highest heats of H_2 adsorption.

Effect of Platinum Loading on H_2 Physisorption

Two sets of MCF-17 samples loaded with platinum were prepared using colloidal synthesis approaches, followed by sonication to infiltrate the nanoparticles (NPs) inside the silica pores. The size distribution was evaluated using TEM imaging (~200 particles were examined in the survey) and ICP-AES elemental analysis was performed to determine the precise amount of metal in the two samples.

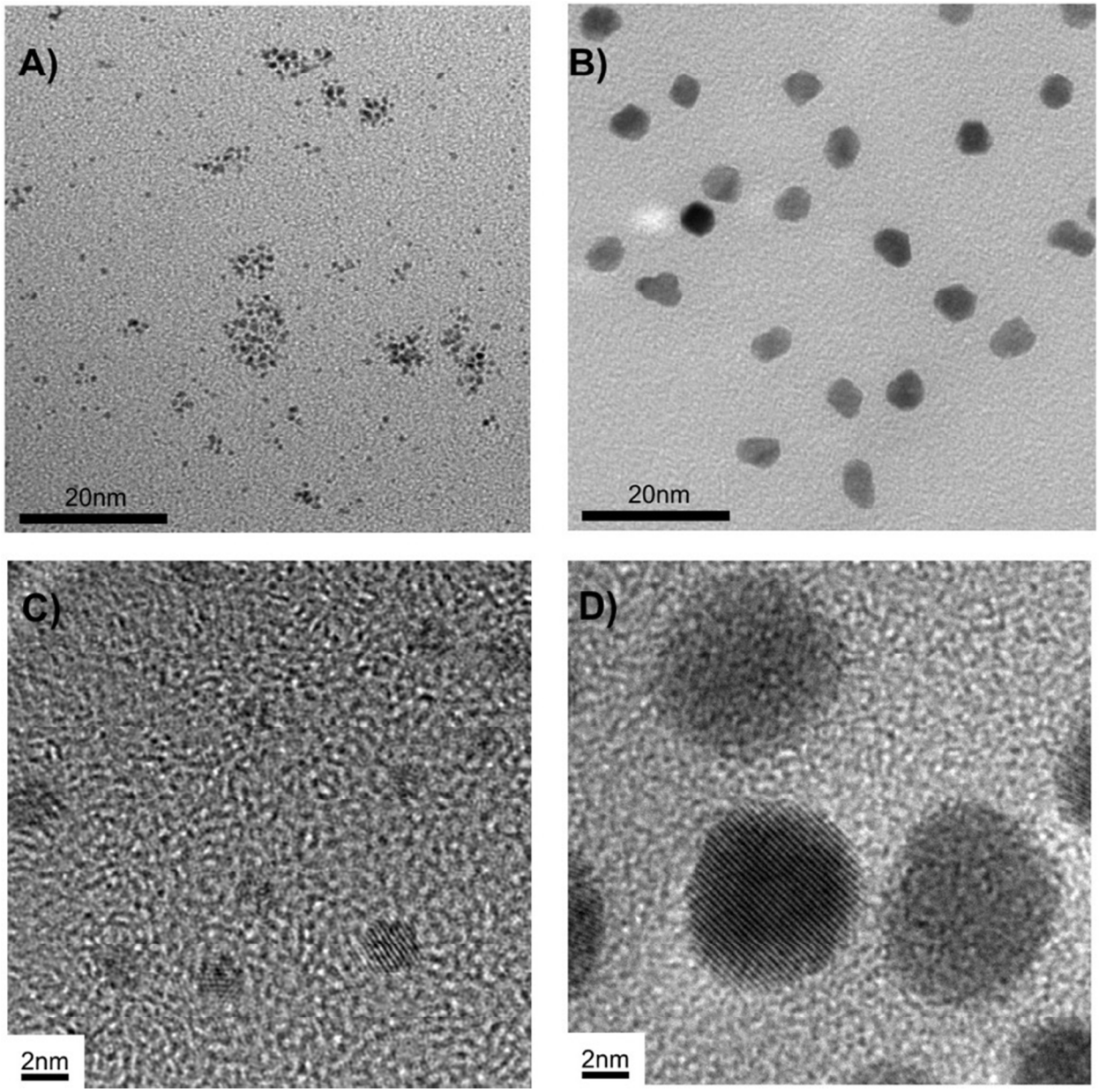

Figure 6. TEM images of platinum nanoparticles: A) 1.5 nm, B) 7 nm, C) high resolution 1.5 nm, and D) high resolution 7 nm.

Table 3 summarizes the characteristics for both samples, Pt-MCF-17-A (with 1.5 nm diameter Pt particles) and Pt-MCF-17-B (with 7.1 nm diameter particles).

Table 3. Physical characteristic of Pt loaded silica samples.

Samples	Support	Pt size nm (σ)	Pt loading (wt.%)
Pt-MCF-17-A	MCF-17	1.5 (±0.3)	0.39
Pt-MCF-17-B	MCF-17	7.1 (±0.9)	0.29

Although the total amount of Pt to be loaded on the sample was aimed to be the same (so as to isolate the effects of nanoparticle size alone), there were nonetheless mass loading discrepancies as the larger particles were more difficult to load into the mesopores of MCF-17 with a pore diameter ~ 16 nm. After a degas under mild conditions (150 ˚C) to prevent excessive sintering of the particles, the samples were both tested for their H_2 adsorption properties. The experiments were performed at liquid N_2 temperature, and the results are shown in Figure 6.

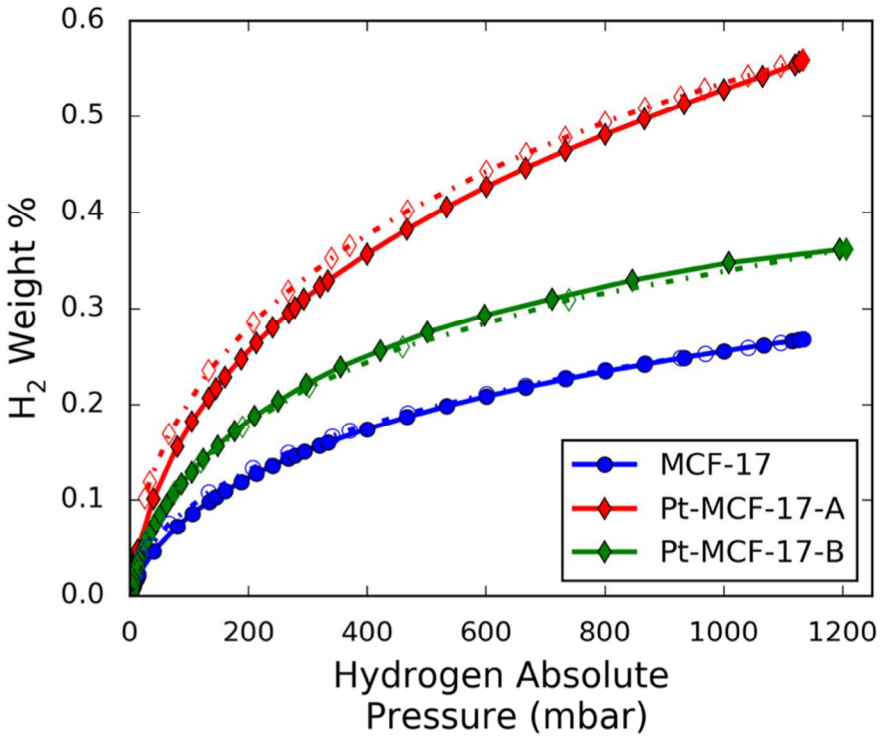

Figure 6. Hydrogen isotherm at liquid nitrogen temperature for platinum loaded samples and mesoporous silica MCF-17.

Using less than 0.4 weight percent (wt.%) of platinum in the sample improves the hydrogen uptake compared to pure MCF-17 at all pressures. In fact, the hydrogen quantity adsorbed per weight of sample corresponds to 0.26 wt.% H for pure MCF-17 and 0.55 wt.%H for MCF-17 loaded with 1.5 nm Pt particles at 1 bar pressure and liquid nitrogen temperature. Overall, the weight penalty arising from the addition of platinum is overcome by the greater improvement in excess hydrogen adsorption. A similar trend is observed for the 7 nm particles, but to a lesser extent (improvement from 0.26 wt.%H to 0.31 wt.%H at 1 bar H_2). To correct for the differences in Pt loading between samples Pt-MCF-17-A and Pt-MCF-17-B, we have normalized the hydrogen uptake curves to their respective platinum mass, with the results shown in Figure 7.

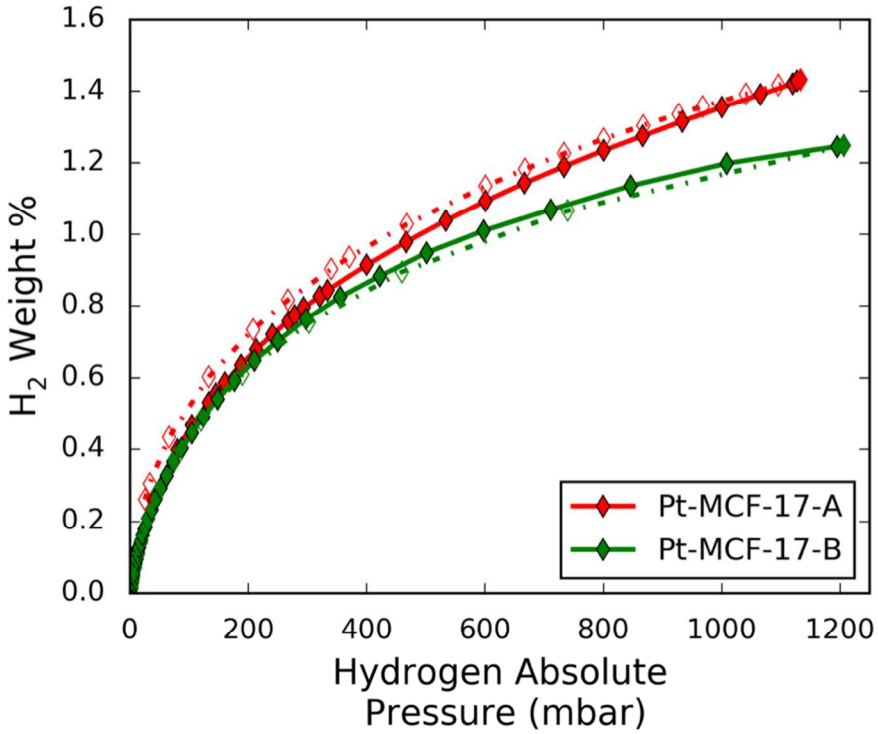

Figure 7. Mass-normalized hydrogen adsorption isotherms for samples containing platinum nanoparticles.

When normalized for the Pt mass, the gain achieved by adding 1.5 nm platinum is still greater than when adding 7.1 nm particles to the sample, and the differences are more significant as the pressure increases. Formation of a Pt hydride is not known to take place under such mild conditions of pressure and temperature, so the increase in hydrogen absorption is not due to Pt reaction with hydrogen. Additionally, the lack of hysteresis between the two steps of the

isotherms (adsorption and desorption) indicate that the improvement is unlikely due to the formation of a platinum hydride.

Our discussion of the enhancement mechanism begins with the reactivity of platinum with hydrogen. Platinum, in many physical forms, is known to dissociate hydrogen, for example bulk Pt(111),[43] stepped Pt surfaces[44] and also as embedded Pt NPs.[45] Hydrogen–deuterium exchange experiments show H-H bond breaking on Pt even at cryogenic temperatures.[43,45] Thermal desorption studies show that the atomic hydrogen produced is relatively thermally stable on Pt, with desorption as H_2 over the range 170 – 420 K for Pt(111).[43,45] Thus, for the cryo H_2 absorption isotherms shown on Figure 6, the Pt NPs are able to dissociate hydrogen, and the hydrogen atoms produced do not desorb from the platinum surface. However, the adsorbed hydrogen atoms are likely to be mobile.

Adsorption directly to platinum cannot by itself account for the Pt-induced H adsorption increase seen in Figure 6. At 1100 mbar, the 1.5 nm diameter Pt particles, with mass loading of 0.39 weight percent, induce an increase in hydrogen adsorption of 0.3 wt. %, or 6.20×10^{-4} grams for the 0.2067 gram Pt/MCF-17 sample. Assuming 80% of the surface area of the 1.5 nm Pt particles is available for hydrogen adsorption (assuming 20% of the surface area is bound to the mesoporous silicate), and taking the H atom saturation coverage for Pt to be 1.2×10^{15} H atoms/cm^2,[43] we calculate that saturation coverage of the 1.5 nm diameter Pt particles can only account for 2.39×10^{-6} grams or 0.385% of the H mass added to the sample at 1100 mbar. Even assuming complete atomic dispersal of Pt in the silicate substrate and assuming formation of a hypothetical hydride with a metal to hydrogen ratio of 1:2, such a scenario can only account for 8.26×10^{-6} grams of H, or 1.33% of the total amount of H added to the Pt-MCF-17-A sample in Figure 6.

Thus, while it very likely that Pt is covered with H at 77 K in the isotherms of Figure 6, that amount of adsorbed hydrogen cannot account for the large increase in hydrogen uptake. The surface area presented by the Pt NPs, combined with the hydrogen pressures (hundreds of mbars) of Figure 6, does allow for a sufficient rate of hydrogen dissociation at the exposed Pt surfaces to generate the H mass increase seen for the experiments of Figure 6. However, the majority of the adsorbed hydrogen cannot reside on Pt for the reasons stated above.

We must therefore consider H diffusion from the Pt NPs to the surrounding MCF-17 silicate substrate at 77 K. It turns out the behavior of hydrogen atoms on silicate surfaces at cryogenic

temperatures is a problem of astrophysical interest.[46-48] It is generally accepted that silicate surfaces, in the form of interstellar dust, are responsible for the production of molecular hydrogen, the most abundant molecule in the interstellar medium. In this process, hydrogen atoms in the vacuum of space are concentrated on silicate dust grains at a temperature of ~ 10 K, where they may diffuse and find each other, desorbing as H_2. It is thought that production of H_2 from H atoms directly in the vacuum has too low a probability to account for the amount of H_2 observed. When a mixed Fe_2SiO_4/Mg_2SiO_4 silicate material is intentionally exposed to beams of atomic H and atomic D at ~ 5K and subsequently warmed to 10 K, the atoms diffuse on the surface and form HD which then desorbs over the temperature range ~ 10 - 25 K. [46-48] Thus, weakly physisorbed H atoms can exist on silicate surfaces when exposed to a source of hydrogen atoms. However, since such weakly physisorbed atoms desorb for temperatures below ~ 25 K, such species cannot be contributing to the hydrogen mass gain seen in the 77 K isotherm of Figure 6. Thus, we believe that for the conditions of Figure 6, most of the atomic H generated at the nanoparticulate Pt surfaces and diffusing onto nearby silicate ends up desorbing from the material, with no net increase in the amount of hydrogen stored in the silicate. In order to register the mass uptake increase in Figure 6, some fraction of the adsorbed H species must be bound in such a way as to be stable at 77 K.

It is possible that hydrogen diffuses from Pt away and into the oxide surface to for an O-H complex within the silicate structure. However, Jing et al.[49] have reported that $(MgFe)SiO_4$, exposed to atomic D at 15 K does not generate D_2O in subsequent thermal desorption, which one might expect to the be produced if O-D moieties were being created by silicate exposure to D atoms. However, it is noteworthy that the model of Cazaux and Tielens[50] of the astrophysical problem explicitly considers the existence of both weakly physisorbed and chemisorbed states of H on silicate. The weakly physisorbed states desorb below 20 K, but the chemisorbed H atoms survive to higher temperatures. It is also noteworthy that Sasamori et al.[51] have directly stabilized atomic H at 300 K in $[(CH_3)_3Si]_8Si_8O_{20}$, which is the trimethylsilylated derivative of the silicate anion.

The diffusion aspect of our speculated mechanism is reasonably supported by prior studies. Conner Jr. et al.[52] showed that hydrogen can diffuse on the surface of carbon in the presence of transition metals such as Pt and Pd. More recently, Karim and co-workers[53] have shown that Pt

NPs can induce H-H bond breaking at 343 K and that the resulting H atoms can diffuse across a TiO_2 support to reduce iron oxide.

The increase in hydrogen uptake seen in Figure 6 cannot be accounted for by a Pt-induced increase in surface area, which would lead to more H_2 molecular binding. We have measured the surface area of Pt/MCF-17 for the 1.5 nm and 7.1 Pt additive and found added Pt reduces the surface area of MCF-17 by 8.2 and 6.4%, respectively. This result is consistent with the well-established findings that metal additives decrease both the specific surface area and the pore volumes of hosts as seen for Pd/C composites,[54] Pd, Pt, Ni and Ru in mesoporous carbon,[55] Pt on AX-21[56] and Pt in microporous carbons.[57,58]

A running controversy in the literature relates to the requirements on the oxide used in supported Pt NPs for the promotion of hydrogen activation and surface transport away from the metal surface. One theory is that the oxide needs to be reducible (e.g. Ti(IV) or other transition metals) to promote transport by providing a driving force for hydrogen to migrate on the oxide surface through a redox reaction involving the metal center. Our experimental results seem to be more consistent with the recent results by Karim *et al*.[53] and suggest that hydrogen can migrate in the vicinity of the Pt particle on non-redox active oxides, such as silica surface.

4. Conclusions

A systematic study of additives was performed to investigate the impact of acidic sites, or the presence of metal particles, on the hydrogen storage properties of mesoporous silica (MCF-17). It was found that the presence of Lewis and Brønsted sites has little effect on the quantity of hydrogen adsorbed. Similarly, the acidic sites have little impact on the hydrogen heat of adsorption. Thus, Lewis and Brønsted acid sites are unable to stabilize hydrogen molecules inside the pores of MCF-17. In contrast, addition of small amounts of Pt nanoparticles significantly improves the storage capacity of MCF-17, up to a factor of two. We found that smaller Pt nanoparticles (1.5 nm diameter) have a greater effect on the hydrogen quantity adsorbed than the larger 7.1 nm diameter Pt particles. In this case, the enhancement in hydrogen storage capacity more than compensated for the weight penalty introduced by adding a high-mass additive such as Pt. As a result, the hydrogen uptake increases by a factor of 2.1, from 0.26 wt.% H for pure MCF-17 to 0.55 wt.%H for MCF-17 loaded with 1.5 nm Pt particles at 1100

mbar. These results are consistent with a recent report by Yin *et al*. on SBA-15 modified with Pt NPs,[59] with the Pt NPs of 3.7 nm displaying higher hydrogen absorption capacity compared to Pt particles of 7.7 nm. This suggests that nanosizing and nanoconfinement can beneficially affect the hydrogen sorption properties of solid-state materials, and could be used as efficient strategies to improve the performance of hydrogen storage materials.

Conflicts of interest

There are no conflicts of interest to declare.

Acknowledgements

The authors acknowledge support through the Hydrogen Storage Materials Advanced Research Consortium of the U.S. Department of Energy (DOE), Office of Energy Efficiency and Renewable Energy, Fuel Cell Technologies Office under Contracts DE-AC52-07NA27344 and DE-AC04-94AL85000. Sandia National Laboratories is a multi-mission laboratory managed by National Technology and Engineering Solutions of Sandia, LLC, a wholly owned subsidiary of Honeywell International Inc., for the DOE's National Nuclear Security Administration under contract DE-NA0003525. The Berkeley work was also supported by the Director, Office of Science, Office of Basic Energy Sciences of the U.S. Department of Energy under Contract No. DE-AC02-05CH11231.

References

1 J. O. Keller, S. Gillie, S. Schoenung, and L. E. Klebanoff. "*The Need for Hydrogen-based Energy Technologies in the 21st Century*," Hydrogen Storage Technology, Materials and Applications. L.E. Klebanoff, Boca Raton: Taylor & Francis; **2012**, p. 3.

2 L. E. Klebanoff, J. O. Keller, M. Fronk, and P. Scott. "*Hydrogen Conversion Technologies and Automotive Applications,"* Hydrogen Storage Technology, Materials and Applications. L.E. Klebanoff, Boca Raton: Taylor & Francis; **2012**, p. 31.

3 H. Barthélémy. *Int. J. of Hydrogen Energy*, 2012, **37**, 17364–17272.

4 S. W. Jorgensen, *Curr. Opinion Solid State Mater. Sci*., 2011, **15**, 39–43.

5 V. Stavila, L. E. Klebanoff, J. J. Vajo, and P. Chen, "*Development of On-Board Reversible Complex Metal Hydrides for Hydrogen Storage*, *Hydrogen Storage Technology, Materials*

and Applications," L.E. Klebanoff, Boca Raton: Taylor & Francis; **2012**, p. 133–212.

6 S. I. Orimo, Y. Nakamori, J. R. Eliseo, A. Zuttel and C. M. Jensen, *Chem. Rev*. 2007, **107**, 4111–4132.

7 J. Graetz, D. J. Wolstenholme, G. P. Pez, L. E. Klebanoff, M. C. McGrady, and A. C. Cooper, "Development of Off-board Reversible Hydrogen Storage Materials," Hydrogen Storage Technology, Materials and Applications. L.E. Klebanoff, Boca Raton: Taylor & Francis; **2012**, p. 239.

8 J. Graetz, *Chem. Soc. Rev*. 2009, **38**, 73–82.

9 B. Chao and L. E. Klebanoff, "Hydrogen Storage in Interstitial Metal Hydrides," Hydrogen Storage Technology, Materials and Applications. L.E. Klebanoff, Boca Raton: Taylor & Francis; **2012**, p. 109.

10 R. C. Bowman and B. Fultz, *MRS Bull.* 2002, **27**, 688–693.

11 C. Ahn and I. Purewal, "Storage Materials Based on Hydrogen Physisorption," Hydrogen Storage Technology, Materials and Applications. L.E. Klebanoff, Boca Raton: Taylor & Francis; **2012**, p. 213.

12 T. Johnson and P. Bénard P., "Solid-State H_2 Storage System Engineering: Direct H_2 Refueling," Hydrogen Storage Technology, Materials and Applications. L.E. Klebanoff, Boca Raton: Taylor & Francis; **2012**, p. 347.

13 G. Petitpas, P. Benard, L. E. Klebanoff, J. Xiao, and S. Aceves, *Int. J. Hydrogen Energy*, 2014, **39**, 10564–10584.

14 B. Bowman, D. Anton, and N. Stetson, *"Engineering Assessments of Condensed-phase Hydrogen Storage Systems,"* Hydrogen Storage Technology, Materials and Applications. L.E. Klebanoff, Boca Raton: Taylor & Francis; **2012**, p. 385.

15 D. A. Sheppard, C. F. Maitland, and C. E. Buckley, *J. Alloys Comp*. 2005, **404-406**, 405–408.

16 M. G. Nijkamp, J. E. M. Raaymakers, A. J. van Dillen, and K. P. de Jong, *Appl. Phys. A*, 2001, **72**, 619–623.

17 J. Dong, X. Wang, H. Xu, Q. Zhao, and J. Li, *Int. J. Hydrogen Energy*, 2007, **32**, 4998–5004.

18 Y. Li and R. T. Yang, *J. Phys. Chem. B* 2006, **110**, 17175–17181.

19 M. Hartmann, C. Bischof, Z. Luan, and L. Kevan, *Microporous Mesoporous Mater*. 2001, **44-45**, 385–394.

20 S. Zheng, F. Fang, G. Zhou, G. Chen, L. Ouyang, M. Zhu, and D. Sun, *Chem. Mater*. 2008, **20**, 3954–3958.

21 R. K. Agarwal, J. S. Noh, J. A. Schwarz, and P. Davini, *Carbon*, 1987, **25**, 219–226.

22 J.S. Noh, R.K. Agarwal and J.A. Schwarz, *Int. J. Hydrogen Energy*, 1987, **12,** 693–700.

23 Y. Li and R.T. Yang, *J. Phys. Chem. C*., 2007, **111**, 11086–11094.

24 R. Campesi, F. Cuevas, R. Gadiou, E. Leroy, M. Hirscher, C. Vix-Guiterla and M. Latroche, *Carbon*, 2008, **46**, 206–214.

25 H.-S. Kim, H. Lee, K.-S. Han, J.-H. Kim, M.-S. Song, M.-S. Park, J.-Y. Lee and J.-K. Kang, *J. Phys. Chem. B*, 2005, **109**, 8983–8986.

26 K. Sabyrov, N. Musselwhite, G. Melaet, and G. A. Somorjai, *Catal. Sci. Technol*., 2017, **7**, 1756–1765.

27 N. Musselwhite, K. Na, S. Alayoglu, and G. A. Somorjai, *J. Am. Chem. Soc.* 2014, **136**, 16661–16665.

28 J. N. Kuhn, C.-K. Tsung, W. Huang, and G. A. Somorjai, *J. Catalysis*, 2009, **265**, 209-215.

29 Y. Han, S. S. Lee, and J. Y. Ying, *Chem. Mater.* 2007, **19**, 2292–2298.

30 G. Melaet, A. E. Lindeman, and G. A. Somorjai, *Top. Catal.* 2014, **57**, 500–507.

31 W.-C. Liu, G. Melaet, W. T. Ralston, S. Alayoglu, Y. Horowitz, R. Ye, and G. A. Samorjai, *Catal. Lett.* 2016, 1–7.

32 K. An, S. Alayoglu, N. Musselwhite, S. Plamthottam, G. Melaet, A. E. Lindeman, and G. A. Samorjai. *J. Am. Chem. Soc*. 2013, **135**, 16689–16696.

33 S. Alayoglu, K. An, G. Melaet, S. Chen, F. Bernardi, L. W. Wang, and G. A. Samorjai. *J. Phys. Chem. C*, 2013, **117**, 26608–26616.

34 V. V. Pushkarev, N. Musselwhite, K. An, S. Alayoglu, and G. A. Somorjai, *Nano Lett*. 2012, **12**, 5196–5201.

35 A. C. Dillon and M. J. Heben, *Appl. Phys. A*, 2001, **72**, 133–142.

36 J. Koresh and A. Soffer, *J. Chem. Soc. Faraday Trans I*, 1980, **76**, 2472–2485.

37 V. B. Kazansky, V. Y. Borovkov, A. Serich, and H. G. Karge, *Microporous Mesoporous Mater*., 1998, **22**, 251–259.

38 S. Tedds, A. Walton, D. P. Broom, and D. Book. *Faraday Discuss*. 2011, **151**, 75–94.

39 B. Schmitz, U. Müller, N. Trukhan, M. Schubert, G. Férey, and M. Hirscher. *Chem. Phys. Phys. Chem*. 2008, **9**, 2181–2184.

40 G. T. Palomino, B. Bonelli, C. O. Arean, J. B. Parra, M. R. L. Carayol, M. Armandi, C. O. Ania, and E. Garrone, *Int. J. Hydrogen Energy*, 2009, **34**, 4371–4378.

41 I. Cabria, M. J. Lopez and J. A. Alonso, *Carbon*, 2007, **45** , 2649–2658.

42 G. Yushin, R. Dash, J. Jagiello, J.E. Fischer and Y. Gogotsi, *Adv. Funct. Mater*. 2006, **16**, 2288–2293.

43 K. Christman, G. Ertl and T. Pignet, *Surf. Sci.* 1976, **54**, 365-392.

44 S.L. Bernasek and G.A. Somorjai, *J. Chem. Phys*. 1975, **62**, 3149-3161.

45 H. Oh, T. Gennett, P. Atanassov, M. Kurttepeli, S. Bals, K.E. Hurst and M. Hirscher, *Microporous Mesoporous Mater*. 2013, **177**, 66-74.

46 V. Pirronello, C.Liu, L. Shen and G. Vidali, *Astrophys. J.* 1997, **475** L69-L72.

47 V. Pirronello, O. Biham, C. Liu, L. Shen and G. Vidali, *Astrophys. J*. 1997, **483**, L131-L134.

48 H.B. Perets, A. Lederhendler, O. Biham, G. Vidali, L. Li, S. Swords, E. Congiu, J. Roser, G.

Manico, J.R. Brucato and V. Pirronello, *Astrophys. J.* 2007, **661**, L163-L166.

49 D. Jing, J. He, J. Brucato, A. De Sio, L. Tozzetti and G. Vidali, Astrophys. J. Lett. 2011, **741**, L9-L13.

50 S. Cazaux and A.G.G.M. Tielens, Astrophys. J. 2002, **575**, L29-L32.

51 R. Sasamori, Y. Okaue, T. Isobe and Y. Matsuda, Science, 1994, **265**, 1691-1693.

52 W.C. Conner Jr., G.M. Pajonk and S.J. Teichner, *Adv. Catal*. 1986, **34** 1-12.

53 W. Karim, C. Spreafico, A. Kleibert, J. Gobrecht, J. VandeVondele, Y. Ekinci, and J.A. van Bokhoven, *Nature*, 2017, **541** 68-73.

54 R. Campesi, F. Cuevas, R. Gadiou, E. Leroy, M. Hirscher, C. Vix-Guterl and M. Latroche, *Carbon*, 2008, **46** 206-214.

55 D. Saha and S. Deng, *Langmuir*, 2009, **25**, 12550-12560.

56 Y. Li and R.T. Yang, *J. Phys. Chem. C*, 2007, **111** 11086-11094.

57 Y.-X. Yang, L. Bourgeois, C. Zhao, D. Zhao, A. Chafee and P.A. Webley, *Microporous Mesoporous Mater*. 2009, **119**, 39-46.

58 A.D. Leuking and R.T. Yang, *Appl. Cat. A: General*, 2004, **265** 259-268.

59. Y. Yin, Z.-F. Yang, Z.-H. Wen, A.-H. Yuan, X.-Q. Liu, Z.-Z. Zhang, H. Zhou**,** *Sci. Rep.,* 2017, **7**, 4509.